Computational Materials Science 47 (2010) 1049–1059

Contents lists available at ScienceDirect

Computational Materials Science

journal homepage: www.elsevier.com/locate/commatsci

Wall thickness and elastic moduli of single-walled carbon nanotubes from frequencies of axial, torsional and inextensional modes of vibration

S.S. Gupta, F.G. Bosco, R.C. Batra *

Department of Engineering Science and Mechanics, M/C 0219, Virginia Polytechnic Institute and State University, Blacksburg, VA 24061, USA

ARTICLE INFO

Article history:
Received 15 July 2009
Received in revised form 15 September 2009
Accepted 1 December 2009
Available online 4 January 2010

Keywords:
Vibrations
Inextensional modes
Equivalent continuum structures
Wall thickness
Elastic moduli

ABSTRACT

Free vibrations of thirty-three armchair, zigzag and chiral single-walled carbon nanotubes (SWCNTs) of aspect ratios (length/diameter) between ~3 and ~15 and having free ends have been studied using the MM3 potential. It is found that these tubes exhibit Rayleigh and Love inextensional modes of vibration. The lowest natural frequency of a mode of vibration corresponds to a circumferential wave number greater than one. Recall that a cylindrical shell of small aspect ratio and comprised of a linear elastic and isotropic material also exhibits the Rayleigh and the Love inextensional modes of vibration. In order to quantitatively compare frequencies of a shell with those of a SWCNT, we find geometric and material parameters for the shell in two ways. In the first approach, we require that the lowest Rayleigh and the radial breathing mode frequencies and the lowest frequencies of the axial and the torsional modes of vibration of a SWCNT match with the corresponding ones of the shell having length and mean diameter equal to those of the SWCNT. In the second technique, we account for the transverse inertia effects, and equate frequencies of the lowest Love, axial and torsional modes of vibration of a SWCNT to that of a shell. Each one of these two methods determines Young's modulus and Poisson's ratio of the material of the shell and its thickness, and enables us to explore similarities and differences between vibrations of a shell and of a SWCNT. It is found that the two techniques give very close results for the material and the geometric parameters of the shell, and hence of the SWCNT. The SWCNT thickness increases from ~0.88 Å to 1.37 Å when the tube radius is increased from ~3.6 Å to 15 Å and stays at 1.37 Å for further increases in the tube radius. The wall thickness is essentially independent of the tube chirality. We use these results to provide an expression for the wall thickness in terms of the tube radius and the bond length in the initial relaxed configuration of a SWCNT.

We also compare higher vibrational modes of shells and hollow cylinders with those of the corresponding SWCNTs. For a shell we use a first-order shear deformable shell theory (FSDST). Frequencies of a shell using the FSDST and of the hollow cylinder using the three-dimensional linear elasticity theory are computed with the finite element method. It is found that for low to moderate circumferential and axial wave numbers frequencies and mode shapes of the shell and of the hollow cylinder agree well with those of the corresponding SWCNT computed with the MM simulations.

1. Introduction

In order to determine elastic constants of a single-walled carbon nanotube (SWCNT) from results of molecular mechanics (MM) simulations or experimental data, one assumes that the response of the SWCNT is equivalent to that of a continuum structure undergoing deformations similar to those of the SWCNT. For a SWCNT, in general, one assumes the length of the equivalent continuum structure (ECS) to be the same as that of the SWCNT being studied. Usually, methods based on continuum theories deliver results whose accuracy depends on assumptions made in deriving a structural model of a SWCNT. For example, using a beam [1–8], a shell [9–18], a hollow cylinder [19], or a solid fiber to study deformations of a SWCNT requires different levels of effort, and yields quite distinct results that may not be close to those found through MM simulations. Furthermore, in structural models, one may simulate a bond between adjoining atoms as a beam, a spring or a truss [5,20,21]. The inherent difficulty here is to determine mechanical properties of the material of the beam, the spring, and the truss from those of the relevant MM/MD potential. Alternatively, one can use the Cauchy–Born rule and the inter-atomic potentials [16] to derive the strain energy density of an elastic body, and then use the three-dimensional (3-D) elasticity theory to analyze initial-boundary-value problems. Most researchers have recognized the ECS of a SWCNT to be a shell or a hollow circular cylinder. One such ECS is shown in Fig. 1. However, finding the thickness h of the annular cross section remains an active area of

* Corresponding author. Tel.: +1 540 231 6051; fax: +1 540 231 4574.
E-mail address: rbatra@vt.edu (R.C. Batra).

0927-0256/$ - see front matter © 2009 Elsevier B.V. All rights reserved.
doi:10.1016/j.commatsci.2009.12.007

research [22], since the SWCNT is 'one carbon atom' thick. We summarize below works that have used either a shell or a hollow cylinder as the ECS of a SWCNT.

Robertson et al. [9] determined elastic properties of graphitic tubules of radii less than 9 Å with the local density functional theory (DFT). For $h = 0.335$ nm, they found that the strain energy relative to the unstrained graphite sheet varies as $1/R^2$ (where R is the radius of the tubule), it is insensitive to tube's chirality, Young's modulus $E = 1.06$ TPa, and the in-plane (in the $z\theta$-plane shown in Fig. 1) stiffness $K(\approx Eh) = \sim 355$ N/m.

Yakobson et al. [10] identified SWCNTs as macroscopic thin elastic shells, derived the bending stiffness $D = Eh^3/12(1-\nu^2) = 0.85$ eV, and $K = 360$ N/m from Robertson et al.'s [9] data of the strain energy due to bending vs. the radius of a tube and the second-order derivative of the strain energy of axial stretching with respect to the axial tensile strain. Poisson's ratio $\nu = 0.19$ for a SWCNT was obtained from the reduction in the diameter of the tube stretched axially in the MD simulations using the Brenner potential. Thus they computed $h = 0.66$ Å and $E = 5.5$ TPa. They studied the buckling of a 6 nm long (7, 7) SWCNT, the bending of an 8 nm long (13, 0) SWCNT and the torsion of a 23 nm long (13, 0) SWCNT using MD simulations with the Brenner potential. Critical points in the strain energy vs. deformation curves for these SWCNTs were found to agree with those obtained from the thin shell theory using values of E and ν found from Robertson et al.'s [9] data.

Wang et al. [11] used values of E and ν computed by Yakobson et al. [10] and found that the relation $G = E/2(1+\nu)$ yields value of the shear modulus significantly higher than that obtained from studying torsional deformations using the Tersoff–Brenner (TB) potential. They thus concluded that the assumption of the shell material being isotropic used by Yakobson et al. [10] may not be valid. *We note that this anomaly may be due to the absence of the potential corresponding to the dihedral torsional degree-of-freedom (the angle ϕ in Fig. 2) in the expression of the TB potential.*

Wang et al. [11] argued in favor of orthotropic symmetry when they found different values of prestrains in the axial and the circumferential directions in the relaxed configurations of SWCNTs in their MD simulations using the TB potential. Though the axial prestrain was found to be negligible and independent of the diameter of a SWCNT, the circumferential prestrain was found to be ~3% for SWCNTs with diameter <1 nm, and both prestrains were negligible for SWCNTs of diameter >1 nm. From the second-order derivatives with respect to appropriate strains of the potential energy due to rolling of a graphene sheet and excess potential energies in the axial tension, the radial deformation and the axial torsion, they computed values of E in the circumferential and the axial directions, the shear modulus and Poisson's ratios for SWCNTs of diameters between ~0.3 nm and ~4 nm. For tubes of diameter >~1.5 nm elastic constants were found to be independent of the tube chirality and the tube diameter, and $E_z = E_\theta = 5.07$ TPa, $G_{\theta z} = 2.19$ TPa and $\nu_{z\theta} = \nu_{\theta z} = 0.165$. Also the converged value of the wall thickness reported by them is

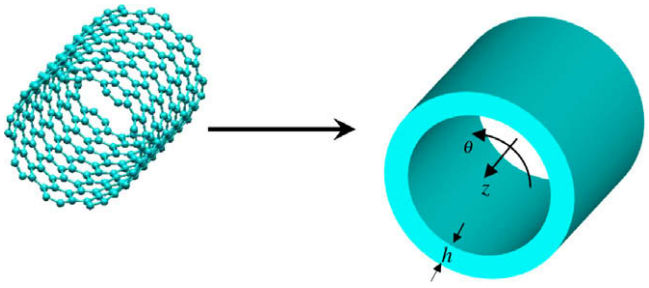

Fig. 1. Equivalent continuum structures of a SWCNT.

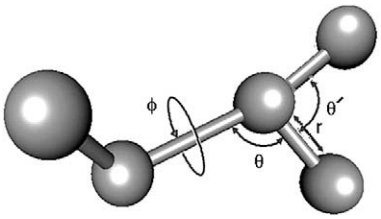

Fig. 2. Depictions of variables r, θ, θ' and ϕ used in the expression for the MM3 potential.

0.0665 nm. Batra and Sears [38] have proposed that the material of the ECS of a SWCNT be modeled as transversely isotropic with the radial line as the axis of transverse isotropy. Their analysis of uniform radial expansion of a SWCNT revealed that for wall thickness of 0.436 Å, values of material moduli are $E_z = E_\theta = 7.26$ TPa, $\nu_{\theta z} = \nu_{z\theta} = 0.21$, $E_r = 5.29$ TPa, and $\nu_{r\theta} = 0.0007$.

Sears and Batra [12] proposed that h for a SWCNT be found by using the relation $E = 2G(1+\nu)$ with E, G, and ν measured in the graphitic plane of a SWCNT. They simulated torsional and axial compressive/tensile deformations of (16, 0) SWCNT using the MM3 potential, and computed ν from changes in the diameter of the tube with an increase in the axial strain. For infinitesimal deformations, they found $\nu = 0.21$, $E = 7.26$ TPa, $G = 3$ TPa, and $h = 0.4593$ Å. However, ν, E and G varied with the strain induced in the tube.

Ru [13] suggested that if $h = 0.34$ nm for a SWCNT is used to compute the bending stiffness D of an elastic shell equivalent to a SWCNT, then D is greater than the 0.85 eV obtained by Yakobson et al. [10]. He further argued that this discrepancy is due to the 'straight normal postulate' of the shell theory. A shell can be divided into several layers and the flexural strains at a point are proportional to the distance of the point from the mid-surface of the shell. This, however, cannot be done for a SWCNT since it is only an atom thick. By computing the critical buckling strain for the SWCNT studied by Yakobson et al. [10], Ru [13] showed that for the shell one should not separate E and h but should work with D.

Wang et al. [14] employed Donnell's and Flügge's shell theories for analyzing buckling deformations and vibrations of ECSs of SWCNTs, and took $D = 0.85$ eV, $K = 360$ N/m and $\nu = 0.2$. Though authors argue that governing equations for an elastic shell employed by them are independent of h, they used 3.4 Å for h to compute the mass density/area of an ECS of a SWCNT from the mass density, 2270 kg/m^3, of bulk graphite. They [14] studied buckling and the frequency regimes of SWCNTs as a combination of the circumferential wave number i and the axial half wave number j but did not compare their results with those from either the MM/MD or the first principle calculations or experimental observations except for the radial breathing mode which corresponds to the strain energy due to stretching deformations. Sears and Batra [38,39] also used these two shell theories to compare buckling deformations of SWCNTs and multi-walled carbon nanotubes with those derived from the shell theories.

Xin et al. [15] calculated strain energies due to rolling, axial compression/stretching, and bending deformations of SWCNTs by considering the total energy of all band electrons. Young's modulus and the effective wall thickness of a SWCNT are obtained from the strain energies due to bending of SWCNTs of various radii and the bending stiffness, D, of a thin shell. They found that E and h for a SWCNT equal 5.1 TPa and 0.74 Å, respectively, and are independent of the radius and the helicity of the tube.

Arroyo and Belytschko [16] modeled a SWCNT as a cylindrical membrane, used the modified Cauchy–Born rule, assumed the membrane material to be hyperelastic, studied twisting and bending deformations of armchair SWCNTs, and obtained a good quantitative and qualitative agreement between deformations of the

membrane and of the corresponding SWCNT. Pantano et al. [17] postulated that stresses are developed when a graphene sheet is rolled into a SWCNT, incorporated these in an FSDST, considered van der Walls (*vdW*) interactions to study the tube/tube, the tube/substrate and the wall to wall interactions in SWCNTs and multi-walled carbon nanotubes, and took $h = 0.75$ Å, $E = 4.84$ TPa. Their analysis of bending deformations of a SWCNT did not reveal effects of *vdW* interactions till the tube locally buckled.

Tu and Ou-Yang [18] derived, in the continuum limit, the energy of a deformed SWCNT from the local density approximation theory, and obtained $h = 0.75$ Å, $E = 4.7$ TPa.

Batra and Gupta [19] used the MM3 potential to compute frequencies of axial, torsional, bending and radial breathing modes of SWCNTs with aspect ratio ≈ 15 and radii ranging from 2 to 10 Å. They equated frequencies of a SWCNT with those of a hollow cylinder by using the 3-D linear elasticity theory and the FEM, and found average values of E and h to equal 3.3 TPa and 1 Å, respectively. Thus $Eh = 54.08$ eV/atom as compared to the 58.2 eV/atom determined by Robertson et al. [9] using the local density functional theory. In Batra and Gupta's [19] work, Poisson's ratio was found to depend on the helicity and the SWCNT radius.

In summary the most often used ECSs of SWCNTs are shell/hollow cylinders with either an assumed value of h or a derived value of h. When the mass of the ECS is set equal to that of carbon atoms in the SWCNT, the value of h affects the mass density of the ECS.

Here we use the MM3 [23] potential to explore physics of free vibrations of relaxed short ($3 <$ aspect ratio $\leqslant 6.0$) and long (aspect ratio $\sim$15) armchair, zigzag and chiral SWCNTs with radii ranging from 4 to 16 Å and ends traction free. The MM3 [23] potential considers bond stretching, the change in angles between adjacent bonds, torsion of the bond, van der Waals forces, and the coupling among stretching, bending and torsional deformations. The energy due to bond stretching has terms that are quadratic, cubic and quartic in the bond length. Thus the strain energy due to bond stretching is not an even function of the change in the bond length.

Results of our MM simulations reveal that vibrations of short SWCNTs with free ends are similar to those of a shell in the sense that both exhibit the Rayleigh and the Love inextensional modes, and the lowest natural frequency occurs for a circumferential wave number greater than one. We determine h, E and ν for shell's material by two alternative methods; first by equating frequencies of the lowest Rayleigh, the radial breathing mode, and the axial and the torsional modes of vibration of a shell with the corresponding ones of a SWCNT computed with the MM simulations. This approach neglects the effect of transverse inertia forces. The second technique considers effects of transverse inertia forces, uses frequencies of the lowest Love, torsional, and axial modes of vibration, and requires solving simultaneously two equations for h and ν. The two techniques give essentially the same values of h and ν.

In order to find a structural model that will replicate well various frequencies and mode shapes of SWCNTs, we have compared the SWCNT frequencies and mode shapes with those of a shell and of a hollow cylinder with geometries of the SWCNT and material properties derived by the procedure stated above. For the shell, we have used a FSDST [24], and deformations of a hollow cylinder have been studied by using the 3-D linear elasticity theory. It is found that for low to moderate circumferential wave numbers the vibrational behavior of the hollow cylinder and the shell using the FSDST agree well with those of the SWCNT derived from the MM simulations.

The remainder of the paper is organized as follows. In Section 2 we describe the MM3 [23] potential, and summarize frequencies of different modes of vibration of a shell in Section 3. In Section 4 we validate our procedure by comparing the presently computed frequencies of the Rayleigh and the radial breathing modes (RBMs) with those available in the literature. Section 5 briefly discusses the effect of the aspect ratio on the Rayleigh, the Love and the radial breathing modes. In Section 6, we find an expression for h as a function of the tube radius by using the least squares method to fit a smooth curve through computed values of h. In Section 7 we find elastic constants of a SWCNT. Section 8 compares the frequency spectrum of a SWCNT with that of the equivalent shell computed by using the FSDST, and of the corresponding hollow cylinder using the 3-D linear elasticity theory. Conclusions of this work are summarized in Section 9.

2. Molecular mechanics simulations

The MM simulations have been performed with the computer code TINKER [25]. The interaction between carbon atoms is specified by using the MM3 [23] potential given by Eq. (1) in which U_s, U_θ and U_ϕ are the primary bond deformation terms accounting, respectively, for the change in the bond length, the change in the angle between adjoining bonds, and the dihedral torsion (the angle ϕ in Fig. 2). The potential U_s has terms that are quadratic, cubic and quartic in the change of bond lengths, and hence is asymmetric with respect to the decrease and the increase in the bond length. U_{vdW} is the potential for the non-bonded van der Waals forces, and its expression involving terms $(r_v/r)^6$ and $\exp(-12r/r_v)$ is different from that in the Lennard–Jones potential; U_{vdW} is negligible for r_v/r greater than 3 where r_v is a material parameter and r the bond length. $U_{s\theta}$ and $U_{\phi s}$ are potentials due to interactions between stretching and bending deformations, and between stretching and twisting deformations. $U_{\theta\theta'}$ represents interactions between different bending modes.

$$
\begin{aligned}
U &= \sum_i \sum_j (U_s + U_\theta + U_\phi + U_{s\theta} + U_{\phi s} + U_{\theta\theta'}) + \sum_i \sum_k U_{vdW},\\
U_s &= 71.94 K_s (r - r_e)^2 \left[1 - 2.55(r - r_e) + \left(\frac{7}{12}\right) 2.55 (r - r_e)^2\right],\\
U_\theta &= 0.021914 K_\theta (\theta - \theta_e)^2 \left[1 - 0.014(\theta - \theta_e) + 5.6(10)^{-5}(\theta - \theta_e)^2 \right.\\
&\quad \left. -7.0(10)^{-7}(\theta - \theta_e)^3 + 9.0(10)^{-10}(\theta - \theta_e)^4\right],\\
U_\phi &= (V_1/2)(1 + \cos\phi) + (V_2/2)(1 - \cos 2\phi) + (V_3/2)(1 + \cos 3\phi),\\
U_{s\theta} &= 2.51118 K_{s\theta}[(r - r_e) + (r' - r'_e)](\theta - \theta_e),\\
U_{\phi s} &= 11.995 (K_{\phi s}/2)(r - r_e)(1 + \cos 3\phi),\\
U_{\theta\theta'} &= -0.021914 K_{\theta\theta'}(\theta - \theta_e)(\theta' - \theta'_e), \text{ and}\\
U_{vdW} &= \varepsilon_e \{-2.25 (r_v/r)^6 + 1.84(10)^5 \exp[-12.0(r/r_v)]\}
\end{aligned}
\tag{1}
$$

Parameters r, θ, θ' and ϕ in Eq. (1) are depicted in Fig. 2. A subscript, e, on a variable signifies its value in the configuration of the minimum potential energy, generally referred to as the relaxed configuration. The total energy of a body equals the sum of potentials of all atoms in the body (indices i and j in Eq. (1) range over bonded atoms, and the index k over all atoms). Values of constants K_s, K_θ, V_1, V_2, V_3, ε_e, r_v, $K_{s\theta}$, $K_{\phi s}$ and $K_{\theta\theta'}$ taken from Ref. [23] are listed in Table 1.

Table 1
Values of parameters in the MM3 potential [23].

Parameter	Value
K_s	4.49 mdyne/Å
K_θ	0.67 mdyne-Å/rad^2
V_1	0.185 kcal/mol
V_2	0.170 kcal/mol
V_3	0.520 kcal/mol
ε_e	0.027 kcal/mol
r_v	2.04 Å
$K_{s\theta}$	0.130 mdyne/rad
$K_{\phi s}$	0.059 mdyne/rad
$K_{\theta\theta'}$	0.24 mdyne-Å/rad^2

A SWCNT is first relaxed to find the minimum energy configuration to within 0.001 kcal/mol/Å rms without using any cut-off distance. Both ends of the tube are taken to be free since there is no ambiguity in simulating these boundary conditions in a laboratory. The module, VIBRATE, in computer code TINKER [25] is used to calculate frequencies. It computes the Hessian of the system by finding second-order derivatives of the MM3 [23] potential with respect to variables appearing in the expression for the potential, and then diagonalizes the mass weighted Hessian to compute eigenvalues and eigenvectors of normal modes.

The first six eigenvalues of the Hessian equal zeros and are discarded since they correspond to three translational and three rotational rigid body modes. The eigenvector associated with an eigenvalue is used to identify the corresponding mode of vibration of a SWCNT. Furthermore, we find one-to-one correspondence between modes of vibration of a SWCNT computed through MM simulations, and those of a linear elastic and isotropic shell [26], and of a linear elastic and isotropic (3-D) hollow cylinder; the latter are computed by using the FEM. For free-free short SWCNTs and shells, some modes of vibration do not involve a change in the axial length; modes of vibration in which deformations do not vary axially are called the Rayleigh modes, and those in which deformations vary linearly in the axial direction are called the Love modes. Both the Rayleigh and the Love modes of vibration generally correspond to the axial half wave number $j = 0$, and are termed inextensional modes. For a circular hollow cylinder this necessitates that generators of the hollow cylinder remain straight during vibration, as shown by the red line in Fig. 3a. Fig. 3b and c show the inextensional Rayleigh and Love modes for (15, 15) SWCNT. The kinematics of inextensional deformations requires that the mid-surface of the SWCNT and of either the shell or the hollow cylinder deform without stretching. The mode of vibration with the circumferential wave number $i = 3$ and the axial half wave number $j = 1$ is shown in Fig. 3d.

3. Expressions for frequencies of different modes of vibration of a shell

We summarize below frequencies of different modes of vibration of a shell comprised of a linear elastic, homogeneous and isotropic material. The reader is referred to Ref. [26] for details of definitions of different modes of vibration, and expressions for their frequencies and mode shapes. For inextensional deformations, the circular natural frequency ω_i^R of a Rayleigh mode of vibration is given by Eq. (2) [26] in which ρ equals the mass density.

$$\omega_i^R = \frac{i(i^2-1)}{\sqrt{(i^2+1)}}\sqrt{\frac{h^2}{12r_e^2}}\left[\frac{1}{r_e}\sqrt{\frac{E}{\rho(1-\nu^2)}}\right]; \quad i = 2,3,4,\ldots \tag{2}$$

For a shell with aspect ratio of at least ~4.0,

$$\omega_{RBM} = \frac{1}{r_e}\sqrt{\frac{E}{\rho(1-\nu^2)}} \tag{2a}$$

where ω_{RBM} equals the frequency of a radial breathing mode of vibration that is identified as a prominent A_{1g} spectral line in the Raman spectroscope of a SWCNT. For aspect ratios < 4.0, ω_{RBM} given by Eq. (2a) has an appreciable error (Ref. [26]).

The thickness of the shell, corresponding to a SWCNT of a minimum aspect ratio of ~4, in terms of ω_i^R and ω_{RBM}, is given by

$$h = \frac{\sqrt{12(i^2+1)}}{i(i^2-1)}\left(\frac{\omega_i^R}{\omega_{RBM}}\right)r_e; \quad i = 2,3,4,\ldots \tag{3}$$

Note that every integer value of i in Eq. (3) must give the same value of h.

The frequency ω_i^L of the Love mode of vibration of a shell of an *arbitrary aspect ratio* is given by Eq. (4) [26] in which l_e equals the length of the shell.

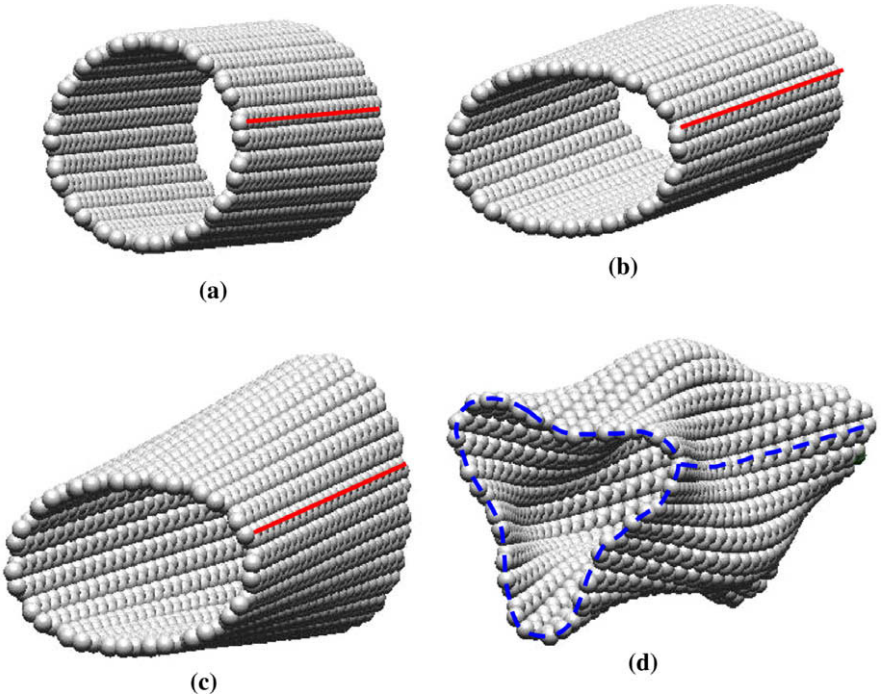

Fig. 3. Modes of vibration of (15, 15) SWCNT of aspect ratio 2.237: (a) tube in the relaxed state, (b) the lowest Rayleigh mode of frequency 11.828 cm^{-1}, (c) the lowest Love mode of frequency 13.119 cm^{-1}, and (d) the mode corresponding to $i = 3$ and $j = 1$ having frequency 40.945 cm^{-1}. A generating line of the cylindrical surface whose length remains unchanged during inextensional vibrations is shown in red color. In Fig. 3d, three circumferential waves and a half axial wave are shown as dashed blue lines for a bending mode of vibration. (For interpretation of the references to color in this figure legend, the reader is referred to the web version of this article.)

$$\omega_i^L = \frac{i(i^2-1)}{\sqrt{(i^2+1)}}\sqrt{\frac{h^2}{12r_e^2}}\left[\frac{1}{r_e}\sqrt{\frac{E}{\rho(1-\nu^2)}}\right]\left[\frac{1+\frac{24(1-\nu)r_e^2}{i^2l_e^2}}{1+\frac{12r_e^2}{i^2(i^2+1)l_e^2}}\right]^{1/2};$$
$$i = 2,3,4,\ldots \tag{4}$$

Eq. (4) implies that with an increase in the aspect ratio the frequency of the Love mode converges to that of the Rayleigh mode.

Frequencies ω_k^A of the axial modes of oscillations of a shell of aspect ratio 4, and ω_k^T of the torsional vibrations of a shell of any aspect ratio, are given, respectively, by

$$\omega_k^A = \frac{k\pi}{l_e}\sqrt{\frac{E}{\rho}}; \quad k = 1,2,3,\ldots \tag{5}$$

$$\omega_k^T = \frac{k\pi}{l_e}\sqrt{\frac{G}{\rho}}; \quad k = 1,2,3,\ldots \tag{6}$$

Since $E = 2G(1+\nu)$, Eqs. (4) and (5) give the following expression for ν:

$$\nu = \frac{1}{2}\left(\frac{\omega_k^A}{\omega_k^T}\right)^2 - 1; \quad k = 1,2,3,\ldots \tag{7}$$

However, for shells of aspect ratio <4, the transverse inertia effects are dominant and frequencies of axial vibrations are given by [27]

$$\omega_k^A = \frac{k\pi}{\sqrt{\left(1+\frac{\nu^2\kappa^2k^2\pi^2}{l_e^2}\right)}}\left[\frac{1}{l_e}\sqrt{\frac{E}{\rho}}\right]; \quad k = 1,2,3,\ldots \tag{8}$$

where κ is the polar radius of gyration. The consideration of transverse inertia decreases the fundamental frequencies of axial vibrations, and the determination of Poisson's ratio from frequencies requires *a priori* knowledge of the geometry of the shell because of the appearance of κ and l_e in Eq. (8). Eq. (8) implies that the frequency of the kth mode does not equal k times the frequency of the first mode of vibration.

The elimination of E from Eqs. (6) and (8) yields the following quadratic equation in ν.

$$\nu^2\left(r_e^2+\frac{h^2}{4}\right)\left[\frac{k\pi\omega_k^A}{l_e\omega_k^T}\right]^2 - 2\nu + \left[\left(\frac{\omega_k^A}{\omega_k^T}\right)^2 - 2\right] = 0; \quad k = 1,2,3,\ldots \tag{9}$$

Similarly, Eqs. (4) and (6) give

$$h^2 = \frac{6(i^2+1)(k\pi)^2r_e^4(1-\nu)}{i^2(i^2-1)^2l_e^2}\left(\frac{\omega_i^L}{\omega_k^T}\right)^2\left[\frac{1+\frac{12r_e^2}{i^2(i^2+1)l_e^2}}{1+\frac{24(1-\nu)r_e^2}{i^2l_e^2}}\right];$$
$$i = k+1; \quad k = 1,2,3,\ldots \tag{10}$$

Eqs. (9) and (10) can be solved simultaneously for ν and h from frequencies of the axial, the torsional and the Love modes of vibration. Whereas Eqs. (9) and (10) incorporate effects of transverse inertia, Eqs. (3) and (7) do not. Substitution for h from Eq. (10) into Eq. (9) yields a cubic equation for ν which has at least one real root. For given values of $\left(\frac{\omega_i^L}{\omega_k^T}\right)$, ν derived from Eqs. (9) and (10) depends upon the slenderness ratio, l_e/r_e. However, $\left(\frac{\omega_i^L}{\omega_k^T}\right)$ depends upon the radius r_e of the tube in the relaxed configuration.

4. Comparison of presently found frequencies with those in the literature

To validate our procedure and the applicability of the MM3 [23] potential to SWCNTs we have listed in Table 2 frequencies, ω_{RBM}

Table 2
Geometries of large aspect ratio SWCNTs, their frequencies from MM simulations, computed Poisson's ratio and wall thickness, and comparison with frequencies of the RBM found by other investigators.

Tube (n,m)	Radius (r_e) (Å)	A.R. (l_e/d_e)	$\omega^R(i=2)$ (cm^{-1})	$\omega^A(k=1)$ (cm^{-1})	$\omega^T(k=1)$ (cm^{-1})	ω_{RBM} (cm^{-1})	ν	h (Å)	Rayleigh and radial breathing mode in literature						
									Rao et al. [28]		Richter and Subbaswamy [29], Saito et al. [30]		Lawler et al. [31]	Kurti et al. [32]	Kuzmany et al. [33] (*experimental*)
									ω^R (cm^{-1})	ω_{RBM} (cm^{-1})					
(10, 0)	3.713	15.200	53.323	29.633	18.732	290.463	0.251	0.879	N.A.	N.A.	N.A.		294	298	N.A.
(9, 6)	4.854	16.279	38.925	20.893	13.622	221.496	0.176	1.101	N.A.	N.A.	N.A.		222	N.A.	N.A.
(8, 8)	5.143	15.086	36.036	21.161	13.833	209.008	0.170	1.144	34	206	N.A.		210	219	211
(9, 9)	5.787	15.023	29.814	18.902	12.319	185.896	0.177	1.198	27	183	N.A.		187	195	195
(16, 0)	5.937	15.263	27.781	18.329	11.633	181.747	0.241	1.172	N. A.	N.A.	N.A.		177	188[a]	185
(10, 10)	6.427	14.971	24.955	17.077	11.101	167.377	0.183	1.237	22	165	165		169	175	177
(11, 11)	7.071	14.930	21.133	15.574	10.103	152.207	0.188	1.267	18	150	N.A.		N.A.	159	162
(20, 0)	7.420	15.021	19.040	14.691	9.346	145.363	0.235	1.255	N.A.	N.A.	N.A.		N.A.	150	N.A.
(22, 7)	9.723	16.337	11.733	10.424	6.682	110.808	0.217	1.329	N.A.	N.A.	N.A.		N.A.	N.A.	N.A.

[a] Obtained from the expression for the RBM proposed by Kurti et al. [32].

Table 3
Geometries of SWCNTs, their frequencies in various modes of vibration from MM simulations; computed wall thickness, Poisson's ratio, Young's modulus; axial and bending stiffnesses; [A.R. = aspect ratio].

Tube (n, m)	Radius (r_e) (Å)	A.R. (l_e/d_e)	ω^R $(i = 2)$ (cm^{-1})	ω^L $(i = 2)$ (cm^{-1})	ω^A $(k = 1)$ (cm^{-1})	ω^T $(k = 1)$ (cm^{-1})	ω_{RBM} (cm^{-1})	v	v^*	h (Å)	h^* (Å)	E (TPa)	G (TPa)	K (J m^{-2})	D (eV)
(10, 0)	3.713	5.628	53.274	53.378	78.882	49.601	290.810	0.265	0.272	0.878	0.856	3.939	1.548	364.179	1.389
(6, 6)	3.859	5.600	53.709	54.047	74.460	49.122	278.450	0.149	0.151	0.961	0.984	3.284	1.427	330.850	1.668
(10, 2)	4.134	5.673	48.434	49.109	70.965	45.308	261.023	0.227	0.232	0.990	0.978	3.465	1.407	358.011	1.780
(12, 0)	4.454	5.677	42.722	44.649	64.835	41.040	242.576	0.248	0.254	1.013	1.042	3.212	1.280	357.679	2.019
(7, 7)	4.501	5.577	43.891	44.146	64.320	42.270	239.020	0.158	0.160	1.067	1.088	2.983	1.286	333.216	2.053
(9, 6)	4.854	5.827	38.889	38.970	56.610	36.923	221.801	0.175	0.178	1.099	1.125	2.867	1.217	333.135	2.193
(10, 5)	4.910	5.289	37.963	38.099	61.939	40.118	219.504	0.192	0.196	1.096	1.113	2.919	1.220	337.841	2.177
(8, 8)	5.143	5.673	35.957	36.160	55.496	36.335	209.323	0.166	0.169	1.140	1.160	2.809	1.201	335.324	2.345
(14, 0)	5.196	5.771	34.241	34.280	54.999	34.762	207.980	0.252	0.258	1.104	1.081	3.107	1.235	359.850	2.188
(11, 7)	5.832	5.333	29.041	29.519	52.028	33.822	185.142	0.183	0.187	1.181	1.212	2.692	1.134	337.926	2.580
(16, 0)	5.937	6.070	27.767	27.799	45.760	28.989	181.960	0.246	0.251	1.170	1.149	2.918	1.166	357.796	2.456
(10, 10)	6.427	5.626	24.893	25.070	44.915	29.242	167.644	0.180	0.183	1.232	1.249	2.618	1.107	338.170	2.742
(15, 4)	6.437	5.445	24.386	24.489	47.302	30.323	167.720	0.217	0.222	1.208	1.188	2.827	1.157	353.129	2.591
(18, 0)	6.679	5.598	22.837	23.283	43.854	27.895	161.773	0.236	0.241	1.217	1.225	2.718	1.095	353.434	2.757
(20, 0)	7.420	5.671	19.011	19.085	39.112	24.856	145.577	0.238	0.244	1.251	1.234	2.704	1.087	354.809	2.811
(19, 2)	7.448	5.717	18.953	19.127	38.941	24.850	145.013	0.228	0.233	1.257	1.241	2.708	1.098	355.233	2.843
(12, 12)	7.711	5.671	18.042	18.193	37.226	24.144	139.778	0.189	0.192	1.285	1.300	2.521	1.058	340.224	2.989
(18, 6)	8.026	5.692	16.670	16.834	36.120	23.204	134.460	0.212	0.216	1.285	1.279	2.606	1.072	349.587	2.974
(16, 12)	9.026	5.685	13.463	13.572	32.105	20.749	119.462	0.197	0.201	1.313	1.310	2.532	1.054	345.706	3.087
(25, 0)	9.274	5.624	12.712	12.797	31.526	20.089	116.439	0.231	0.237	1.307	1.296	2.568	1.038	352.516	3.079
(15, 15)	9.638	5.624	11.959	12.087	30.091	19.448	111.878	0.197	0.201	1.330	1.343	2.445	1.018	342.187	3.212
(22, 7)	9.723	5.689	11.702	11.820	29.869	19.171	110.990	0.214	0.218	1.323	1.316	2.535	1.040	350.157	3.153
(30, 0)	11.129	5.683	9.046	9.125	25.991	16.590	97.013	0.227	0.232	1.340	1.333	2.493	1.011	351.147	3.244
(18, 18)	11.565	5.644	8.468	8.572	25.028	16.143	93.253	0.202	0.206	1.356	1.368	2.403	0.997	343.466	3.346
(25, 10)	11.583	5.684	8.416	8.515	25.022	16.076	93.153	0.211	0.216	1.351	1.350	2.461	1.012	348.330	3.300
(30, 5)	12.162	5.677	7.652	7.746	23.894	15.301	88.750	0.219	0.224	1.354	1.349	2.468	1.008	350.590	3.319
(33, 0)	12.241	6.239	7.551	7.562	21.542	13.758	87.507	0.226	0.230	1.364	1.340	2.479	1.008	350.719	3.275
(20, 20)	12.850	5.669	6.916	7.006	22.444	14.462	83.935	0.204	0.208	1.367	1.379	2.387	0.988	344.110	3.404
(36, 0)	13.354	5.669	6.396	6.492	21.668	13.863	80.834	0.222	0.226	1.364	1.370	2.417	0.985	348.998	3.407
(36, 5)	14.372	5.443	5.548	5.634	21.099	13.518	75.118	0.218	0.223	1.370	1.368	2.434	0.995	350.441	3.410
(24, 24)	15.419	6.009	4.858	4.920	17.678	11.374	69.941	0.208	0.211	1.383	1.394	2.366	0.977	345.164	3.487
(43, 0)	15.950	6.052	4.528	4.579	17.035	10.895	67.653	0.222	0.227	1.378	1.378	2.407	0.981	349.654	3.453
(33, 16)	16.053	5.443	4.482	4.554	18.866	12.122	67.221	0.211	0.216	1.382	1.383	2.401	0.988	348.374	3.468

Table 4
Geometries of SWCNTs, their frequencies from MM simulations in various modes of vibration, computed Poisson's ratio and wall thickness. Entries in columns 11 and 14 equal, respectively, differences between v and v^*, and between h and h^*.

Tube (n, m)	Radius (r_e) (Å)	A.R. (l_e/d_e)	ω^R $(i = 2)$ (cm^{-1})	ω^L $(i = 2)$ (cm^{-1})	ω^A $(k = 1)$ (cm^{-1})	ω^T $(k = 1)$ (cm^{-1})	ω_{RBM} (cm^{-1})	v	v^*	|% Diff.|	h (Å)	h^* (Å)	|% Diff.|
(10, 0)	3.713	4.087	53.121	53.574	103.353	64.841	291.131	0.270	0.286	5.754	0.874	0.885	1.262
(6, 6)	3.859	4.088	53.463	54.581	100.818	66.650	278.903	0.144	0.148	2.603	0.954	0.990	3.734
(10, 2)	4.134	4.156	47.730	49.478	92.206	59.298	261.333	0.209	0.217	3.959	0.974	1.023	4.981
(12, 0)	4.454	4.009	42.551	42.953	91.644	57.675	242.977	0.262	0.277	5.755	1.007	0.980	2.623
(7, 7)	4.501	4.022	43.705	44.584	88.233	58.110	239.456	0.153	0.157	2.885	1.060	1.093	3.126
(9, 6)	4.854	5.829	38.889	38.970	56.610	36.923	221.801	0.175	0.178	1.564	1.098	1.124	2.380
(10, 5)	4.910	5.290	37.963	38.099	61.939	40.118	219.504	0.192	0.196	2.130	1.096	1.112	1.495
(8, 8)	5.143	3.972	35.804	36.557	78.425	51.465	209.754	0.161	0.166	3.152	1.133	1.164	2.779
(14, 0)	5.196	4.214	34.143	34.423	74.864	47.275	208.276	0.254	0.266	4.922	1.099	1.074	2.277
(11, 7)	5.832	4.248	29.027	29.631	66.554	43.341	185.076	0.179	0.185	3.109	1.181	1.181	0.000
(16, 0)	5.937	4.026	27.657	27.986	68.478	43.357	182.333	0.247	0.260	5.248	1.163	1.141	1.864
(10, 10)	6.427	4.083	24.811	25.334	61.385	40.043	167.956	0.175	0.181	3.277	1.226	1.253	2.221
(15, 4)	6.437	4.283	24.357	25.135	58.997	37.858	167.922	0.214	0.222	3.806	1.205	1.228	1.901
(18, 0)	6.679	4.183	22.744	23.017	58.631	37.202	162.018	0.242	0.253	4.679	1.210	1.192	1.531
(20, 0)	7.420	4.581	18.951	19.122	48.262	30.659	145.720	0.236	0.248	3.780	1.246	1.228	1.427
(19, 2)	7.448	4.572	18.917	19.377	48.033	30.668	145.158	0.227	0.235	3.541	1.253	1.262	0.687
(12, 12)	7.711	3.704	17.965	18.516	56.408	36.693	140.184	0.182	0.189	4.224	1.276	1.307	2.454
(18, 6)	8.026	4.489	16.621	16.902	45.370	29.153	134.617	0.211	0.218	3.363	1.279	1.283	0.247
(16, 12)	9.026	4.044	13.412	13.821	44.659	28.907	119.708	0.193	0.201	3.771	1.306	1.327	1.618
(25, 0)	9.274	4.098	12.675	12.920	43.056	27.455	116.649	0.230	0.240	4.559	1.301	1.294	0.549
(15, 15)	9.638	3.930	11.924	12.274	42.753	27.695	112.137	0.191	0.199	3.958	1.324	1.350	2.040
(22, 7)	9.723	3.556	11.651	12.080	46.666	30.041	111.354	0.207	0.218	5.432	1.314	1.342	2.158
(30, 0)	11.129	4.321	9.024	9.202	34.059	21.755	97.159	0.225	0.234	3.961	1.335	1.332	0.192
(18, 18)	11.565	4.181	8.448	8.679	33.606	21.713	93.185	0.198	0.205	3.601	1.354	1.374	1.477
(25, 10)	11.583	3.934	8.394	8.653	35.611	22.928	93.365	0.206	0.215	4.331	1.345	1.368	1.700
(30, 5)	12.162	3.763	7.633	7.913	35.484	22.784	88.992	0.213	0.223	4.971	1.347	1.371	1.775
(20, 20)	12.850	3.218	6.806	7.006	39.077	25.305	85.996	0.192	0.204	6.174	1.313	1.349	2.717
(36, 0)	13.354	4.200	6.377	6.534	29.160	18.657	80.576	0.221	0.231	4.099	1.364	1.361	0.267
(36, 5)	14.371	4.082	5.540	5.722	28.078	18.020	75.259	0.214	0.223	4.183	1.366	1.372	0.487

(in cm^{-1} = Hertz/speed of light in cm/s), of radial breathing modes (A_{1g} symmetry mode) of long SWCNTs (aspect ratio ~15) computed from MM simulations, and those given in Refs. [28–33]. Of these the ones from Ref. [33] are experimental values. Rao et al. [28] computed the lowest frequency of the E_{2g} symmetry mode for (8, 8), (9, 9), (10, 10) and (11, 11) SWCNTs using the C–C force constants optimized to fit the experimental phonon dispersion for a flat graphene sheet. However, they did not observe these modes in their experiments on the four SWCNTs very likely due to the scattering of waves. These E_{2g} symmetry modes are the Rayleigh inextensional modes corresponding to $i = 2$ for long SWCNTs, and their frequencies and mode shapes compare well with those found in our MM simulations for tubes with aspect ratio of ~15. Thus the MM3 potential represents well deformations of SWCNTs in the radial breathing mode.

5. Comparison of frequencies of the Rayleigh and the Love modes

In Tables 3 and 4 we have listed for the thirty-three (11 zigzag, 9 armchair, and 13 chiral) SWCNTs, the tubes' geometries, and the lowest frequencies of the Rayleigh, the Love, the axial, the torsional, and the radial breathing modes. Whereas results in Table 3 are for tubes with aspect ratio of ~6, those in Table 4 are for tubes of aspect ratio between 3 and 6 and radii ranging from 4 to 15 Å. For these SWCNTs, frequencies of the lowest Rayleigh and the lowest Love modes differ by less than 1%. However, for the (20, 0) SWCNT having an aspect ratio ~1.0, the lowest Rayleigh mode frequency is 17.99 cm^{-1} while the lowest Love mode frequency equals 23.998 cm^{-1} indicating the transverse inertia effects, but, for the same SWCNT of aspect ratio ~5.67, these two frequencies equal 19.011 cm^{-1} and 19.085 cm^{-1} respectively; cf. row 15 of Table 3.

Gupta and Batra [34] used the MM3 potential and the computer code TINKER to compute radial breathing mode frequencies of SWCNTs having aspect ratio of ~15, and found that the ω_{RBM} and the radius r_e satisfy $\omega_{RBM} = 1076\ (cm^{-1})/r_e$. Values of ω_{RBM} listed in Tables 3 and 4 lie on the curve $\omega_{RBM} = 1071\ (cm^{-1})/r_e$. Thus the relation between ω_{RBM} and r_e is unaffected by the aspect ratio of a SWCNT.

6. Thickness of single-walled carbon nanotubes

Assuming that a SWCNT can be represented as a shell or a 3-D hollow cylinder, we set the length and the mean radius of the shell equal to the length l_e and the radius r_e of the SWCNT in the relaxed configuration. We find the wall thickness h of the shell and hence of the SWCNT from either Eq. (3) or Eq. (10). The wall thickness h determined from Eq. (3) using frequencies of radial breathing and Rayleigh modes derived from the MM simulation results is independent of values of E, ρ and ν, but may depend upon the radius of the SWCNT or of the shell. However, the wall thickness h^* determined by simultaneously solving Eqs. (9) and (10) may depend upon Poisson's ratio ν^*. For the 33 SWCNTs studied here, tubes' geometries (radii, aspect ratios in relaxed configurations) and frequencies of the first axial and the first torsional modes, the first Rayleigh and the first Love modes, the radial breathing mode, and values of h and ν obtained from Eqs. (3) and (7) respectively, and of h^* and ν^* computed by solving Eqs. (9) and (10) simultaneously are listed in Tables 3 and 4. It is evident that Poisson's ratio of a SWCNT computed from Eq. (7) differs from that obtained by solving Eqs. (9) and (10) by less than ~6% for aspect ratios between 3 and 5.5, and by about 1.3% for aspect ratios of ~6. The difference in the wall thickness computed from Eqs. (3) and (10) decreases with an increase in the SWCNT radius, and the maximum difference between the two values is 5%.

For SWCNTs of aspect ratio >4, the transverse inertia effects are negligible and h and ν can be computed from Eqs. (3) and (7); these values are listed in Table 3. A comparison of values listed in Tables 3 and 4 reveals that the two sets of values of h and ν agree well

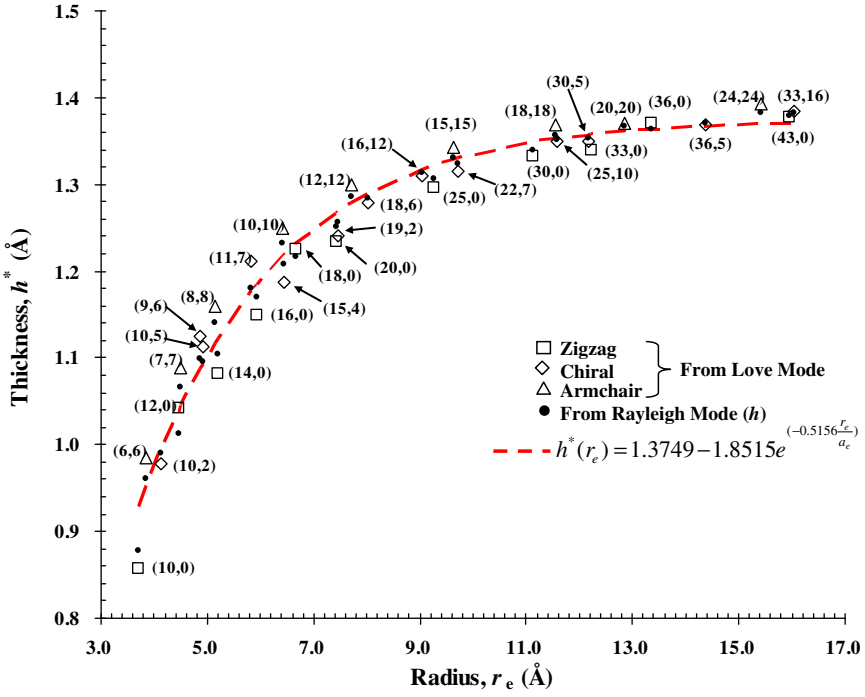

Fig. 4. Dependence upon the tube radius of the wall thickness h^* of zigzag, chiral and armchair relaxed SWCNTs. The wall thickness h computed from Eq. (3) is shown by a dot. The red dashed curve is obtained by the least squares fit to the computed values. (For interpretation of the references to color in this figure legend, the reader is referred to the web version of this article.)

with each other. For some SWCNTs considered in Table 3 and 4 but now of aspect ratio ~15, values of the wall thickness computed from the Rayleigh mode are listed in Table 2. From Tables 2–4 it can be concluded that over the range of aspect ratios from ~3 to ~15, values of the wall thickness of the SWCNTs are independent of the aspect ratio but depend upon the tube radius.

In Fig. 4, we have plotted the variation of the thicknesses h^* and h of a SWCNT with its radius r_e in the relaxed configuration. These results show that for the same radius the thickness of an armchair tube is the largest and that of a zigzag tube the smallest, and the thickness of a chiral tube has an intermediate value. The exponential function

$$h^*(r_e) = 1.3749 - 1.8515e^{\left(-0.5156\frac{r_e}{a_e}\right)} \tag{11}$$

fitted through the data by the least squares method is shown as a red dashed curve in Fig. 4. In Eq. (11) a_e is the equilibrated bond length (1.346 Å). For $r_e < 7.5$ Å, Eq. (11) gives the SWCNT thickness that differs from its value derived from Eq. (2) or Eq. (6) by less than 4% except for the (10, 0) SWCNT that has a difference of ~8%. For 15 Å > r_e > 7.5 Å the difference in values of h^* and h is between 1% and 1.5%. For $r_e > 15$ Å, the exponential term in Eq. (11) equals essentially zero, and the thickness has a nearly uniform value of 1.37 Å that is independent of tube's chirality. Recalling that $r_e = 1.1026\ a_e\ (m^2 + n^2 + mn)^{1/2}$, Eq. (11) can be written in terms of the lattice vector parameters (m, n). Eq. (11) *coupled with expressions for frequencies of a shell will enable designers to compute natural frequencies of a nano-mechanical resonator rather quickly and select an appropriate SWCNT for a particular application. If desired, the selection can be refined by using the computationally intensive ab initio or MM simulations.*

We note that computed values of h for all 33 SWCNTs of different chiralities are less than the diameter 1.42 Å of a carbon atom which complies with the Vodenitcharova–Zhang proposal [35] that the wall thickness be less than the diameter of a carbon atom.

7. Elastic constants of single-walled carbon nanotubes

In Table 3 we have listed values of Young's modulus E computed from Eq. (8) using values of the wall thickness h^* and Poisson's ratio ν^*. Values of Poisson's ratio determined from Eqs. (7) and (9) are also listed in Tables 3 and 4. The mass density ρ^* of the shell and the hollow cylinder material is found from

$$\rho^* = \frac{m_c n_c}{2\pi r_e h^* l_e} \tag{12}$$

where m_c is the mass (1.992×10^{-26} kg) of a carbon atom, and n_c equals the number of carbon atoms in the SWCNT. Whereas values found from Eqs. (8)–(10) are valid for SWCNTs of all aspect ratios, those from Eqs. (3), (5), and (7) are generally valid for tubes of aspect ratio 4. Values of both E and G depend upon the tube radius and converge to 2.4 TPa and 1.0 TPa, respectively, as the tube radius is increased to 15 Å. For the lowest radius (10, 0) SWCNT considered in these simulations, E = 4.0 TPa, and G = 1.55 TPa.

We note that Poisson's ratios ν and ν^* of SWCNTs vary with the tube radius and depend upon tube's helicity. In Fig. 5 values of ν and ν^* for SWCNTs listed in Tables 3 and 4 are plotted against the tube radius in the relaxed configuration. It is found that, in general, for a given radius of a SWCNT the value of Poisson's ratio is the highest for a zigzag tube and the lowest for an armchair tube. With an increase in the radius of a SWCNT, the value of Poisson's ratio appears to converge to 0.218 for tubes of all helicities. Poisson's ratios of zigzag and armchair SWCNTs vary rather smoothly with a change in their radii but those of chiral SWCNTs do not lie on a smooth curve. Sanchez-Portal et al. [36] computed Poisson's ratio from *ab initio* calculations and reported a similar trend. Gupta and Batra [34] studied vibrations of free-free SWCNTs of aspect ratio ~15 and also found a trend similar to that shown in Fig. 5 for Poisson's ratio, and it converged to 0.20, 0.21 and 0.23 for armchair, chiral and zigzag tubes.

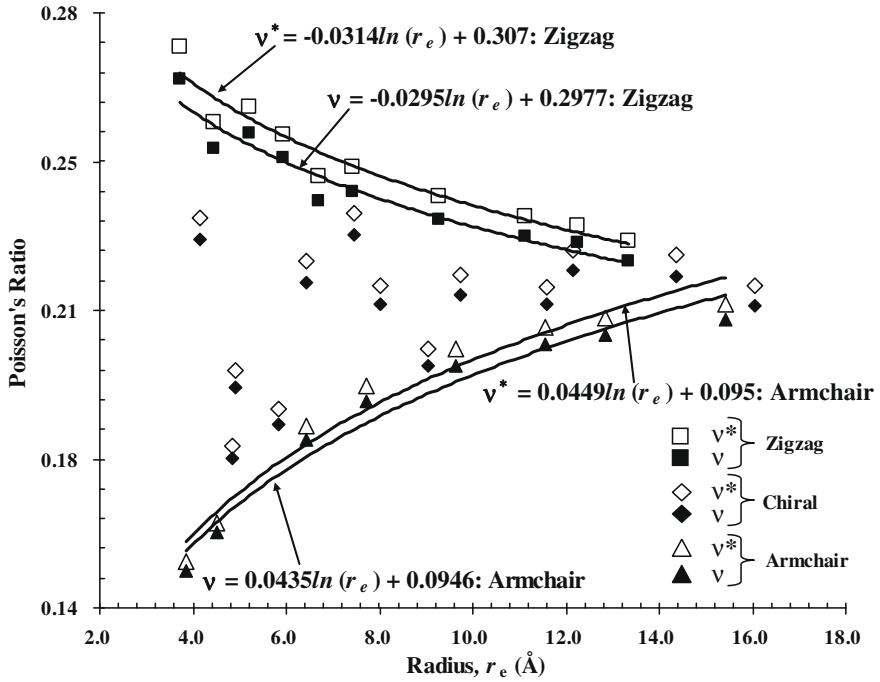

Fig. 5. Variation of Poisson's ratio with the radius of a relaxed SWCNT. Poisson's ratio computed from Eqs. (9) and (10) is represented by open squares, triangles and diamonds while that computed from Eq. (7) is represented by filled squares, triangles and diamonds. Expressions of least squares fits to data for values of Poisson's ratio for armchair and zigzag tubes computed from the two approaches are shown; r_e in these expressions is in Å. For chiral tubes a smooth curve could not be fitted through the computed values.

Table 5
Frequencies of various vibrational modes, and values of elastic moduli of (36, 5) SWCNT for simulations with structural models.

SWCNT (m, n) n_c	Aspect ratio (l_e/d_e)	#	Torsional mode (cm^{-1})	Axial mode (cm^{-1})	Love mode ($i = 2$) (cm^{-1})	Rayleigh mode ($i = 2$) (cm^{-1})	Thickness (h^*) (Å)	Poisson's ratio ν^*	Young's modulus (E) TPa
(36, 5) 6004	5.443	1	13.518	21.099	5.634	5.548	1.368	0.223	2.434
		2	27.033	41.813					

n_c: No. of carbon atoms in MM simulations.
#: Mode no.

We have also given in Table 3 computed values of the axial stiffness, K, and of the bending stiffness, D. The axial stiffness is found to vary with the tube radius, and for a given tube radius it is the highest for a zigzag tube and the lowest for a chiral tube. The average value of K equals 347.52 J/m^2 which is about 3.46% less than the 360 J/m^2 reported in Ref. [22]. The bending stiffness is found to vary between 1.4 eV and 3.5 eV; it increases with an increase in the tube radius and converges to 3.5 eV. As mentioned in the Introduction, Robertson et al.'s [9] data gives $D = 0.85$ eV, $K = 360$ J/m^2, and $\nu = 0.19$. This rather low value of D resulted in Yakobson et al.'s [10] getting $h = 0.66$ Å.

8. Comparison of natural frequencies of SWCNT with those of a shell and a hollow cylinder

We now compare frequencies of different modes of vibration of an arbitrarily chosen (36, 5) SWCNT having aspect ratio 5.443 determined through MM simulations with those of a shell and a 3-D linear elastic hollow cylinder found by using the FEM and the commercial computer code ABAQUS [37]. The shell and the hollow cylinder materials are taken to be linear elastic, homogeneous and isotropic with values of material parameters equal to those of the corresponding SWCNT found above. Table 5 lists values of various material parameters needed to compute natural frequencies and corresponding mode shapes.

For the shell we use the FSDST [24] with the shear correction factor of 5/6. However, 3-D deformations of the hollow cylinder are analyzed. When using the FSDST [24], the FE mesh for the shell is comprised of 8-node shear deformable elements (S8R) and is refined successively till the computed frequencies have converged to 0.01% of their values. The hollow cylinder is divided into 20-node brick elements (C3D20R) and the FE mesh is refined to obtain converged values of frequencies. The FE meshes for a shell and a hollow cylinder that gave converged frequencies are listed in Table 6.

Frequencies of SWCNTs computed through MM simulations, and of the shell and the hollow cylinder computed with the FEM are given in Table 7 and are plotted in Fig. 6 to depict the variation of the frequency for various axial half wave numbers with the circumferential wave number. In Fig. 6, results from the MM simulations overlap those from the FSDST [24] and the analysis of the hollow cylinder. We compare in Table 7 frequencies of modes (i, j) for the (36, 5) SWCNT with those of the shell and the hollow cylinder. It is clear that frequencies of inextensional and bending modes of the hollow cylinder for all circumferential and axial wave numbers agree very well with those of the SWCNT with the maximum difference between any two corresponding values being 1.28%. For a shell, the FSDST [24] gives frequencies that differ from the corresponding MM results

Table 6
FE meshes yielding converged frequencies during the modal study of shear deformable shell and hollow cylinder models of (36, 5) SWCNT employing the computer software ABAQUS.

Tube	No. of 20-node brick elements[a]		No. of 8-node shell elements	
	Along the circumference	Along the axis	Along the circumference	Along the axis
(36, 5)	45	74	46	78

[a] One element in the thickness direction.

Table 7
Comparison of frequencies of various modes of vibration of (36, 5) SWCNT found from MM simulations with those of the shell using the FSDST and of the hollow cylinder using the 3-D linear elasticity theory.

Axial half wave number	SWCNT		(36, 5)				
	Circumferential wave number		1 (cm^{-1})	2 (cm^{-1})	3 (cm^{-1})	4 (cm^{-1})	5 (cm^{-1})
1		MM	8.235	6.697	16.161	30.266	48.281
	|% Error| w.r.t. MM	3D-FEM	0.069	1.108	0.572	0.872	1.275
		FSDST	0.006	1.338	0.951	1.389	1.950
2		MM	17.943	10.075	17.246	31.063	48.976
	|% Error| w.r.t. MM	3D-FEM	0.153	0.724	0.706	0.858	1.141
		FSDST	0.073	0.907	1.084	1.383	1.825
3		MM	28.038	15.434	19.218	32.325	50.081
	|% Error| w.r.t. MM	3D-FEM	0.285	0.418	0.883	0.936	1.150
		FSDST	0.199	0.572	1.242	1.467	1.844
4		MM	36.833	21.659	22.164	34.115	51.619
	|% Error| w.r.t. MM	3D-FEM	0.302	0.170	1.019	1.068	1.282
		FSDST	0.217	0.308	1.346	1.600	1.983
Inextensional modes							
Rayleigh mode		MM	–	5.548	15.592	29.550	46.766
	|% Error| w.r.t. MM	3D-FEM	–	0.623	0.625	0.332	0.745
		FSDST	–	0.871	0.995	0.844	0.064
Love mode		MM	–	5.634	15.642	29.570	46.971
	|% Error| w.r.t. MM	3D-FEM	–	0.638	0.260	0.038	0.519
		FSDST	–	0.885	0.635	0.554	0.162

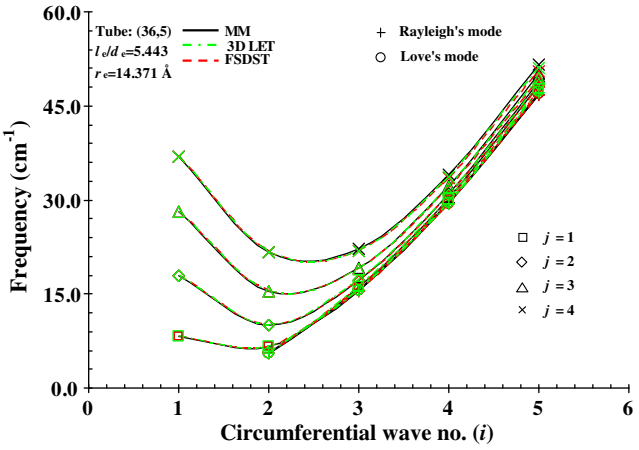

Fig. 6. Variation with the circumferential wave number of the bending and the inextensional mode frequencies of (36, 5) SWCNT found from MM simulations, of the shell obtained by using the FSDST and of the hollow cylinder. Results from the MM simulations overlap those from the FSDST and the analysis of the hollow cylinder.

by at most 1.98%. Frequencies of the (36, 5) SWCNT for moderate values of the circumferential and the axial wave numbers, plotted in Fig. 6, show that the lowest natural frequency does not correspond to $j = 1$ and $i = 1$ as would be the case if the SWCNT were modeled as a beam, but corresponds to $i = 2$ for the first four axial half wave numbers. For $j = 3$ and 4, the lowest frequency in Fig. 6 occurs for $2 < i < 3$ because of the smooth curve plotted through the data. The knowledge of this lowest frequency is important in tuning a resonator during the sweep of frequencies from low to high values. Calculations based on modeling a SWCNT as a beam will overestimate fundamental frequencies of the SWCNT. However, SWCNTs of large aspect ratios may have the lowest natural frequency corresponding to $j = 1$ and $i = 1$. Furthermore, the MM simulation results reveal that with an increase in the circumferential wave number, frequencies of bending modes of vibration approach those of the inextensional modes which generally holds for a shell made of a linear elastic isotropic material.

9. Remarks

Subsequent work [40] on SWCNTs has shown that for a free-free zig-zag (n, 0) SWCNT, frequencies of inextensional modes of vibration saturate at a circumferential wave number of either $(n-1)/2$ or $n/2$ for odd and even values of n. However, this does not occur both for a thin shell and a hollow cylinder. Thus all results obtained by using a structural theory may not correspond with those of SWCNTs as is often assumed.

10. Conclusions

Vibrations of thirty-three free-free SWCNTs of aspect ratios between ~3 and ~15 have been studied through MM simulations using the MM3 potential. In order to compare the frequency spectrum of a SWCNT with that of a shell, the thickness of a SWCNT/shell is derived by equating analytical frequencies of the lowest inextensional either Love or Rayleigh, torsional and axial modes of a shell to those of a SWCNT found through MM simulations. The wall thickness of a SWCNT is found to increase with an increase in its radius and converges to 1.37 Å for SWCNTs of radii >15 Å. Thus SWCNTs of radii exceeding 15 Å have the same wall thickness of 1.37 Å which is slightly smaller than the diameter, 1.42 Å, of a carbon atom. The functional relationship between the tube thickness and its radius has been derived by fitting a smooth curve through the computed data by the least squares method.

Vibration modes of a SWCNT computed through MM simulations have been compared with those of a shell whose length and mean diameter equal, respectively, those of the relaxed SWCNT. Frequencies of the shell have been computed with the first-order shear deformation shell theory and by regarding the SWCNT as a three-dimensional hollow cylinder comprised of an isotropic linear elastic material. Frequencies of the shell and the hollow cylinder are determined by the finite element method. It is found that for first four axial half waves and up to six full circumferential waves vibration modes of a SWCNT from MM simulations agree well with those of the equivalent shell and hollow cylinder.

For the design of very high frequency nano-resonators, this work provides a useful tool to accurately predict the lowest natural frequency of a SWCNT by using a computationally less expensive structural model.

Acknowledgements

This work was supported by the Office of Naval Research Grant N00014-06-1-0567 to Virginia Polytechnic Institute and State University with Dr. Y.D.S. Rajapakse as the program manager. Views expressed in the paper are those of authors, and neither of the funding agency nor of their institutions.

References

[1] K. Sohlberg, B.G. Sumpter, R.E. Tuzun, D.W. Noid, Nanotechnology 9 (1998) 30–36.
[2] N. Yao, V. Lordi, J. Appl. Phys. 84 (1998) 1939–1943.
[3] A. Krishnan, E. Dujardin, T.W. Ebbesen, P.N. Yianilos, M.M.J. Treacy, Phys. Rev. B 58 (1998). Art. No. 14013.
[4] P. Poncharal, Z.L. Wang, D. Urarte, W.A. de Heer, Science 283 (1999) 1513–1516.
[5] C. Li, T.W. Chou, Appl. Phys. Lett. 84 (2004) 121–123.
[6] J. Yoon, C.Q. Ru, A. Mioduchowski, J. Appl. Mech. 72 (2005) 10–17.
[7] P.M. Agrawal, B.S. Sudalayandi, L.M. Raff, R. Komanduri, Comput. Mater. Sci. 38 (2006) 271–281.
[8] Q. Wang, V.K. Varadan, Int. J. Solids Struct. 43 (2006) 254–265.
[9] D.H. Robertson, D.W. Brenner, J.W. Mintmire, Phys. Rev. B 45 (1992) 12592–12595.
[10] B.I. Yakobson, C.J. Brabec, J. Bernholc, Phys. Rev. Lett. 76 (1996) 2511–2514.
[11] L. Wang, Q. Zheng, J.Z. Liu, Q. Jiang, Phys. Rev. Lett. 95 (2005). Art. No. 105501.
[12] A. Sears, R.C. Batra, Phys. Rev. B 69 (2004). Art. No. 235406.
[13] C.Q. Ru, Phys. Rev. B 62 (2000) 9973–9976.
[14] C.Y. Wang, C.Q. Ru, A. Mioduchowski, J. Appl. Mech. 71 (2004) 622–631.
[15] Z. Xin, Z. Jianjun, O.Y. Zhong, Phys. Rev. B 62 (2000) 13692–13696.
[16] M. Arroyo, T. Belytschko, J. Mech. Phys. Solids 50 (2002) 1941–1977.
[17] A. Pantano, D.M. Parks, M.C. Boyce, J. Mech. Phys. Solids 52 (2004) 789–821.
[18] Z. Tu, Z. Ou-Yang, Phys. Rev. B 65 (2002). Art. No. 233407.
[19] R.C. Batra, S.S. Gupta, J. Appl. Mech. 75 (2008). Art. No. 061010.
[20] T. Natsuki, K. Tantrakarn, M. Endo, Carbon 42 (2004) 39–45.
[21] M. Mir, A. Hosseini, G.H. Majzoobi, Comput. Mater. Sci. 43 (2008) 540–548.
[22] Y. Wang, L.C. Zhang, Nanotechnology 19 (2008). Art. No. 75705.
[23] N.L. Allinger, Y.H. Yuh, J. H Lii, J. Am. Chem. Soc. 111 (1998) 8551–8566.
[24] S.P. Timoshenko, S. Woinowsky-Krieger, Theory of Plates and Shells, second ed., McGraw-Hill, New York, 1959.
[25] J.W. Ponder, Computer Code TINKER MOLECULAR MODELLING PACKAGE 4.2, 2004.
[26] R.D. Blevins, Formulas for Natural Frequencies and Mode Shapes, Van Nostrand Reinhold Company, New York, 1979.
[27] A.W. Leissa, J. So, J. Acoust. Soc. Am. 98 (1995) 2122–2135.
[28] A.M. Rao, E. Richter, S. Bandow, B. Chase, P.C. Eklund, K.A. Williams, S. Fang, K.R. Subbaswamy, M. Menon, A. Thess, R.E. Smalley, G. Dresselhaus, M.S. Dresselhaus, Science 275 (1997) 187–191.
[29] E. Richter, K.R. Subbaswamy, Phys. Rev. Lett. 79 (1997) 2738–2741.
[30] R. Saito, T. Takeya, T. Kimura, G. Dresselhaus, M.S. Dresselhaus, Phys. Rev. B 57 (1998) 4145–4153.
[31] H.M. Lawler, D. Areshkin, J.W. Mintmire, C.T. White, Phys. Rev. B 72 (2005). Art. No. 233403.
[32] J. Kurti, G. Kresse, H. Kuzmany, Phys. Rev. B 58 (1998) R8869.
[33] H. Kuzmany, B. Burger, M. Hulman, J. Kurti, A.G. Rinzler, R.E. Smalley, Europhys. Lett. 44 (1998) 518–524.
[34] S.S. Gupta, R.C. Batra, Comput. Mater. Sci. 43 (2008) 715–723.
[35] T. Vodenitcharova, L.C. Zhang, Phys. Rev. B 68 (2003). Art. No. 165401.
[36] D. Sanchez-Portal, E. Artacho, J.M. Soler, Phys. Rev. B 59 (1999) 12678–12688.
[37] User's Manual Finite Element Computer Code ABAQUS 6.6.
[38] A. Sears, R.C. Batra, Phys. Rev. B 73 (2006). Art. No. 085410.
[39] R.C. Batra, A. Sears, Model. Simul. Mater. Sci. Eng. 15 (2007) 835–844.
[40] S.S. Gupta, F. Bosco, R.C. Batra, J. Appl. Phys. 106 (2009). Art. No. 063527.